J Sol-Gel Sci Technol (2016) 79:107–113
DOI 10.1007/s10971-016-4017-0

ORIGINAL PAPER: NANO-STRUCTURED MATERIALS (PARTICLES, FIBERS, COLLOIDS, COMPOSITES, ETC.)

Self-propagating combustion synthesis and synergistic photocatalytic activity of $GdFeO_3$ nanoparticles

Li Li[1,2] · Xiong Wang[1]

Received: 25 October 2015 / Accepted: 14 March 2016 / Published online: 21 March 2016

Abstract $GdFeO_3$ (GFO) nanoparticles were synthesized by a glycine-assisted self-propagating combustion process. The as-synthesized $GdFeO_3$ was characterized by X-ray diffraction, transmission electron microscopy, and UV–Vis diffuse reflectance spectra. The visible-light-responsive photocatalytic activity of $GdFeO_3$ nanoparticles was evaluated by the photodegradation of Rhodamine B under visible light. The results indicate that the as-prepared $GdFeO_3$ nanoparticles exhibit remarkable visible-light photocatalytic activity through the synergism of semiconductor-photocatalyzed oxidation and heterogeneous Fenton-like reaction. Compared with the bulk GFO, the photodecomposition rate of RhB was improved about 22 times when the simultaneous presence of the nanoparticles and H_2O_2 was observed. The mechanism and the main active species involved in photocatalytic oxidative reaction were also investigated through the carriers trapping experiments.

Graphical Abstract

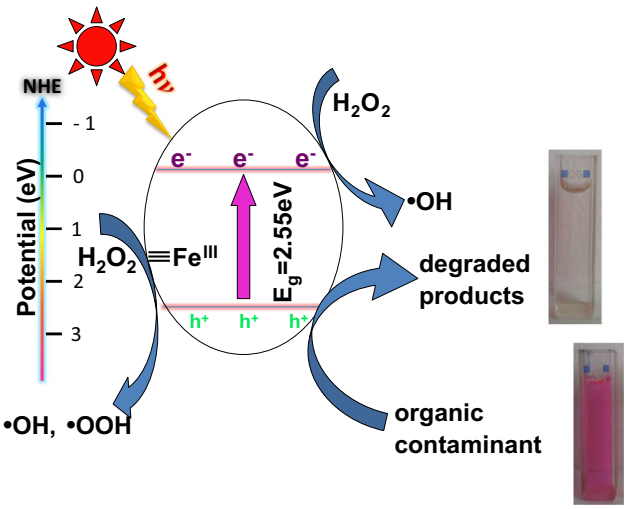

Keywords $GdFeO_3$ · Nanoparticle · Glycine-assisted combustion · Photocatalyst · Photo-Fenton-like

1 Introduction

In recent years, photocatalysis processes have been intensively investigated for wastewater treatment [1, 2]. The photocatalytic oxidation has also been proposed as an effective method for treatment of toxic and polluted water [3, 4]. Up to date, the researches on photocatalysis have mostly focused on TiO_2-based photocatalysts with a crystalline modification of anatase (Degussa P25, Hombriat UV-100, Aldrich, etc.) as a result of their high photocatalytic activity and widespread uses for large-scale water

✉ Xiong Wang
xiongwang@mail.njust.edu.cn; xiongwang@njust.edu.cn

[1] School of Materials Science and Engineering, Nanjing University of Science and Technology, Nanjing 210094, China

[2] School of Chemical and Materials Engineering, Huainan Normal University, Huainan 232038, China

treatment. However, a major drawback of TiO_2 is that only UV in the solar spectrum (about 3–5 %) can be utilized to initiate the photocatalytic redox processes because of the large band gaps of anatase TiO_2 (3.2 eV) and rutile TiO_2 (3.0 eV) [5–7] so that the effective utilization of solar energy is limited. To increase the utilization efficiency of sunlight and improve the photocatalytic activity, novel visible-light-driven photocatalysts with high activity and stability must be developed [8, 9].

Rare-earth orthoferrite compounds $LnFeO_3$ (Ln = lanthanide elements) constitute a very important class of materials due to their antiferromagnetism and magnetooptic effects [10, 11]. They generally crystallize in the orthorhombic perovskite structure in which the FeO_6 octahedra get distorted to the extent decided by the size of rare-earth ions. They have potential for various applications such as solid oxide fuel cells, sensors, magnetooptic materials, electrode materials, catalysts, and magnetic resonance imaging (MRI) in biomedicine [12–15]. Recently, rare-earth orthoferrite compounds with perovskite structure [16–19], such as $SmFeO_3$, $LaFeO_3$, $GdFeO_3$, $EuFeO_3$, $NdFeO_3$, $PrFeO_3$, and $YFeO_3$, have received increasing attention and been applied as photocatalysts. More importantly, it is interesting to note that some perovskite-type Fe-based materials have been confirmed as heterogeneous Fenton-like catalysts. Ju et al. [20] reported that $EuFeO_3$ nanoparticles could activate H_2O_2, yielding a removal of 71 % of RhB with 3 h in the $EuFeO_3/H_2O_2$ system. Sun et al. [21] found that the flower-like $Bi_2Fe_4O_9$ nanoparticles could be used as heterogeneous Fenton-like catalysts.

Various synthesis routes to rare-earth orthoferrites have been proposed, including the precipitation method, thermal decomposition process, solvothermal treatment, sonochemical approach, and combustion route [22–24]. Self-propagating combustion synthesis is a simple, fast, and inexpensive process [25], in which exothermic reaction can generate a large quantity of heat rapidly leading to the formation and crystallization of orthoferrite nanoparticles.

In this paper, nanocrystalline $GdFeO_3$ (GFO) was prepared via a self-propagating combustion method. The structure, morphology, and UV–Vis diffuse reflection spectrum (DRS) of the as-prepared samples were examined. The photocatalytic activity of the nanocrystalline $GdFeO_3$ was also evaluated by the degradation of Rhodamine B under visible-light irradiation. On the basis of the calculated energy band positions and the active species during photocatalytic process, a mechanism of the photocatalysis was proposed and discussed.

2 Experimental

2.1 Synthesis of $GdFeO_3$

The $GdFeO_3$ nanoparticles were synthesized by a glycine-assisted self-propagating combustion technique. All the reagents were of analytical grade and were used as received without further purification.

In a typical synthesis, stoichiometric amounts of gadolinium nitrate hexahydrate ($Gd(NO_3)_3{\cdot}6H_2O$, 5 mmol) and ferric nitrate nonahydrate ($Fe(NO_3)_3{\cdot}9H_2O$, 5 mmol) were dissolved in 50 mL of distilled water. And then glycine (NH_2CH_2COOH, 10 mmol) was added to the solution under stirring. After magnetic stirring for 2 h at 80 °C, a brownish red colloidal sol was obtained. The sol was placed on hot plate and heated. At the initial stage, the sol was condensed, underwent dehydration and decomposition process followed by the evolution of large amount of gases. After a while, it began to burn with the release of much heat instantly. The whole condensation–combustion process took only about 20 min on the hot plate. Finally, the as-prepared sample was washed with distilled water and absolute alcohol for several times and dried at 80 °C. The brown yellow sample was obtained eventually. For comparison, the bulk $GdFeO_3$ was prepared by a traditional solid state method according to the Ref. [26].

2.2 Characterization of samples

The phases of the samples were examined by X-ray diffraction (XRD) on a Bruker D8 Advanced diffractometer. The patterns were collected using unfiltered Cu K_α radiation and the Bragg–Brentano geometry over the 2θ range 20°–70°. The morphology of the as-prepared sample was observed by transmission electron microscopy (TEM, Hitachi, Model H-800, accelerating voltage 200 kV). The infrared spectrum was recorded using Fourier transformed infrared spectroscopy (FT-IR: Model 883, Perkin-Elmer Optoelectronics Inc., USA). UV–Vis DRS result of the sample was obtained on a Shimadzu UV2450 UV–Vis spectrophotometer with an integrating sphere.

2.3 Photocatalysis test

The equipment for photocatalytic reaction is self-designed. The visible-light source was a 500 W Xe lamp (light intensity = 600 mW/cm^2, 20 cm above the solution surface) positioned in a quartz cold trap which was in the middle of multiposition cylindrical reaction vessel. The system was cooled by wind and water and maintained at room temperature. Appropriate cutoff filters were placed

around the cold trap to completely remove radiation below 400 nm, ensuring that the catalysis of the RhB/GFO system occurred only under visible light.

In the experiment, 30 mg $GdFeO_3$ was added to 30 mL RhB solution (10^{-5} mol L^{-1}) in a vessel. Before illumination, the suspensions were stirred in the dark for 30 min to ensure the establishment of an adsorption–desorption equilibrium between the photocatalyst and RhB. Then, the solution was exposed to visible-light irradiation under stirring. At given time intervals, a small quantity of suspension was sampled and centrifuged to remove the photocatalyst particles. The supernatants were analyzed by monitoring the absorbance at 553 nm using the UV–Vis spectrophotometer. To further enhance the photocatalytic performance of $GdFeO_3$ nanoparticles, 1 mL of 3 % H_2O_2 was added to initiate the reaction. After each photocatalytic reaction, the aqueous solution was centrifuged to recycle $GdFeO_3$ nanoparticles that were then dried at 80 °C for the recycling test.

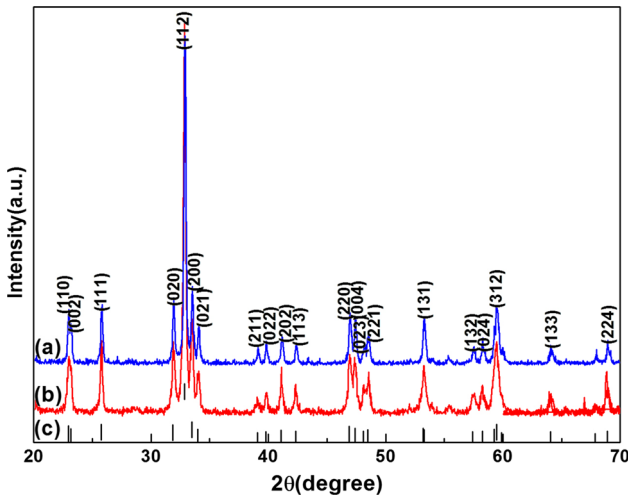

Fig. 1 XRD pattern of the (*a*) synthesized samples and (*b*) bulk GFO; (*c*) standard reflection lines from JCPDS: 47-0067

3 Results and discussion

The purity and crystallinity of the as-synthesized product were examined by powder XRD analysis. As shown in Fig. 1, it can be concluded that both the obtained sample and the bulk GFO synthesized by the traditional solid state method are pure-phase perovskite $GdFeO_3$ and well crystallized with orthorhombic structure with lattice parameters of $a = 5.3647$, $b = 5.6100$, and $c = 7.6537$ Å [space group: *Pbnm*(62)], which are in excellent accordance with the standard data (JCPDS NO.: 47-0067). No other characteristic peaks for impurities were detected, such as Gd_2O_3 and $Gd_3Fe_5O_{12}$. [27]. The average grain size of the sample estimated by Scherrer equation is about 43 nm.

The as-synthesized nanostructures were analyzed by TEM and HRTEM as shown in Fig. 2. As shown in Fig. 2a, it was clear that the particles exhibit an average diameter of about 58 nm with narrow size distribution, which was larger than the value calculated from the XRD pattern that due to agglomeration of GFO particles. The HRTEM image and the associated fast Fourier transform (FFT) of the nanoparticles are shown in Fig. 2b, confirming single-crystalline structure. The 0.383- and 0.273-nm lattice spacings correspond to the (002) and (112) planes of the orthorhombic $GdFeO_3$, respectively, and the angle measured between these two planes is about 45°, which is in good agreement with the calculated value.

The UV–Vis DRS of $GdFeO_3$ is shown in Fig. 3. The curve shows a broad absorption band in the wavelength ranging from 400 to 600 nm, which indicates that $GdFeO_3$ particles can absorb considerable amounts of visible light, implying their potential applications as visible-light-driven photocatalysts [28]. Depending on the Kubelka–Munk formula [29], the relationship between the absorption coefficient and the band-gap energy follows the formula: $(F(R)E)^{n/2} = A(E - E_g)$, in which E and E_g are photon energy and optical band-gap energy, respectively, and A is the characteristic constant of semiconductors. From the

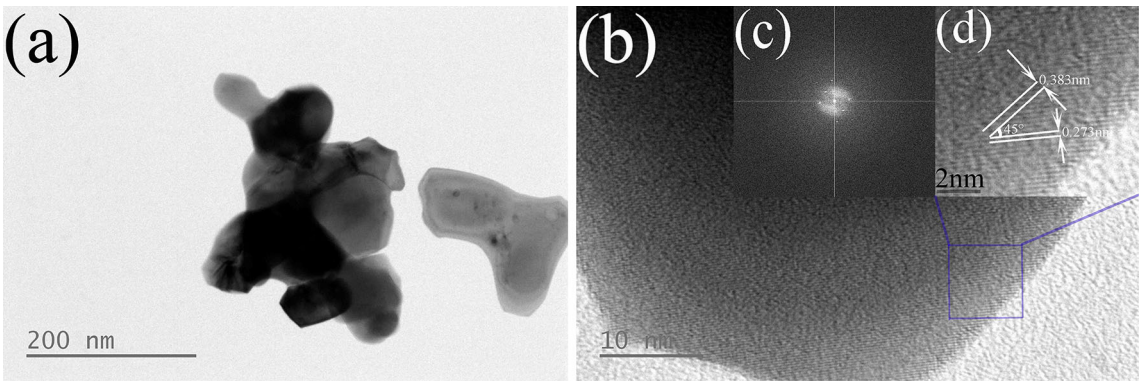

Fig. 2 **a** TEM and **b** HRTEM images of the GFO photocatalyst. The corresponding FFT (**c**) and high magnification images (**d**)

equation, $(F(R)E)^{n/2}$ has a linear relation with E. $GdFeO_3$ is an indirect-gap semiconductor [13], So $n = 4$. The inset of Fig. 3 shows that extrapolating the linear relation as $(F(R)E)^2 = 0$ gives the band-gap E_g of approximately 2.53 and 2.13 eV for the sample and the bulk, respectively, which is quite comparable with other rare-earth orthoferrites [30, 31]. The larger the band gap of the semiconductor, the stronger the redox ability of the photoexcited electron–hole pairs [32]. The larger band gap of the sample induces to a higher photocatalytic activity under visible-light illumination.

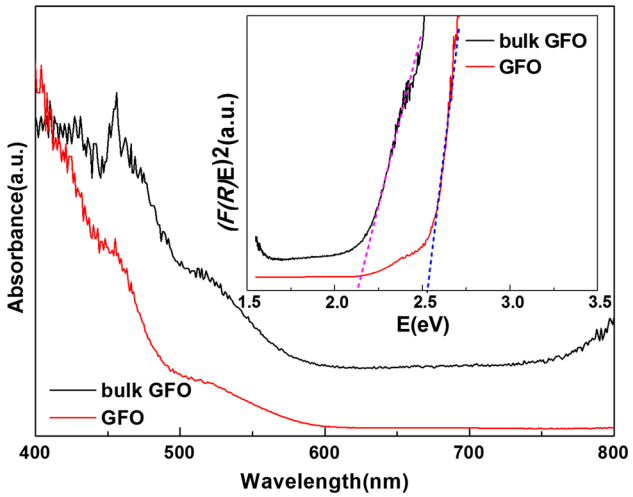

Fig. 3 UV–Vis DRS of the GFO photocatalyst (*inset* shows the estimated band gap by the Kubelka–Munk function)

According to the empirical equation [33, 34]: $E_{VB} = -\chi - E_e + 0.5E_g$, where χ is the absolute electronegativity of $GdFeO_3$, and E_e is the energy of free electrons on the hydrogen scale, and the valence band edge top (E_{VB}) and the conduction band bottom (E_{CB}) of GFO can be determined as 2.435 and −0.115 eV, respectively. Obviously, $GdFeO_3$ is easily excited to photoinduced electron–hole pairs under visible light ($\lambda > 400$ nm) in heterogeneous photocatalysis.

The photocatalytic activity of the $GdFeO_3$ nanoparticles was evaluated by the degradation of the typical organic contaminant RhB under visible-light illumination. The time-dependent photodegradation of RhB over GFO was illustrated in Fig. 4a. GFO nanoparticles exhibit certain

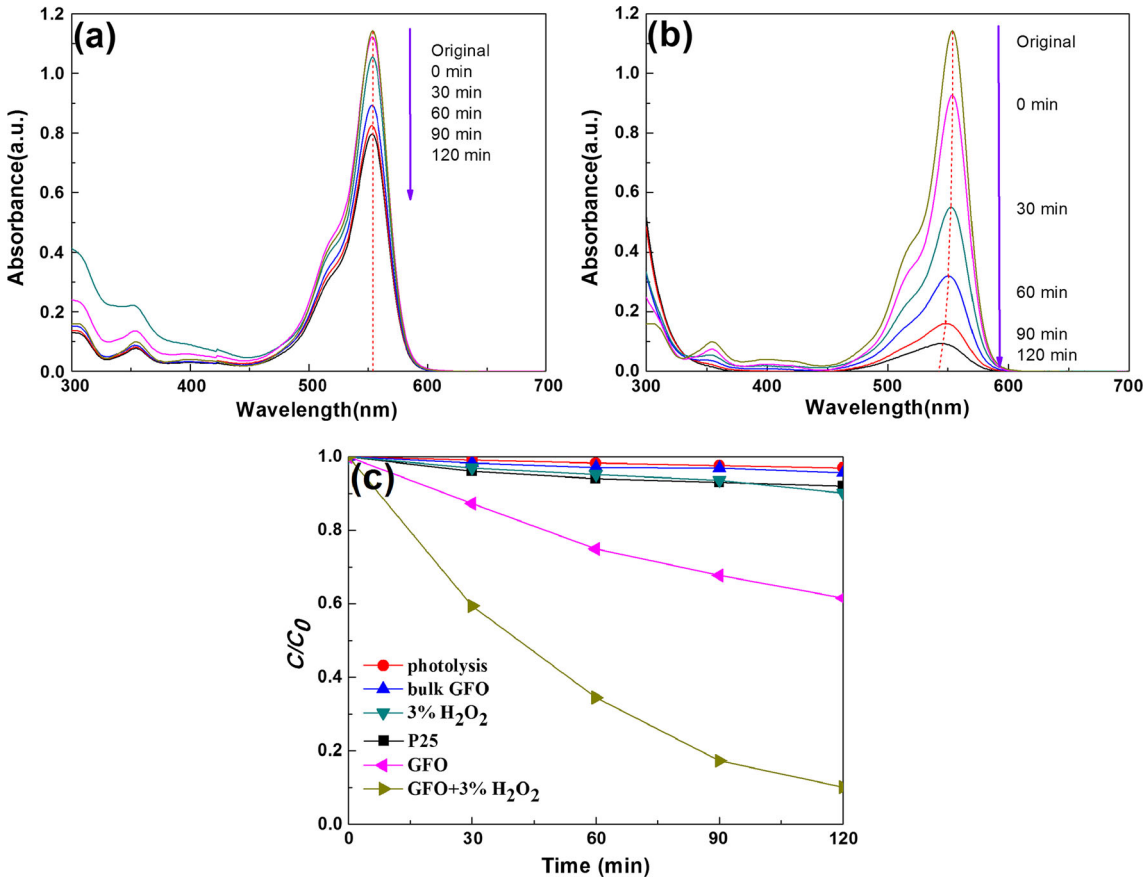

Fig. 4 The evolutions of **a** RhB and **b** RhB + H_2O_2 absorption spectra observed in the presence of GFO photocatalyst at different irradiation times; **c** photogradation efficiencies of RhB as a function of irradiation time at different conditions

extent photocatalytic ability, and 40 % of RhB was decomposed after 2-h illumination, which was better than the bulk and the commercial P25. After adding H_2O_2 into GFO/RhB suspension (Fig. 4b), RhB was dramatically degraded. After 2-h visible-light illumination, the degradation efficiency can reach above 89.9 % (Fig. 4c). It can be seen that the addition of H_2O_2 can obviously accelerate the photocatalytic degradation of RhB. Moreover, the absorption band occurred with slight hypochromatic shift, corresponding to the step-by-step deethylation process of RhB [35], which indicates that the hydroxylation/oxidation of RhB is a predominant procedure [36].

As reported before, nanoscaled iron-based compounds can catalyze the activation of H_2O_2 to produce $^{\cdot}OH$ radicals through Fenton-like reaction, leading to the enhanced degradation of organic contaminants [37–39]. The main Fenton-like process could be depicted as below:

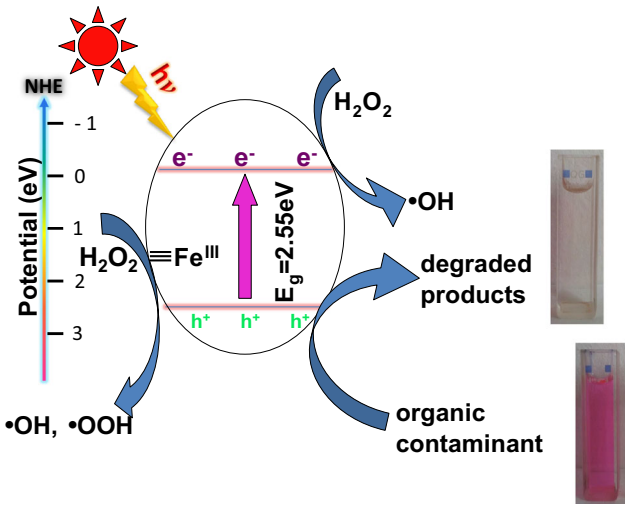

Fig. 5 Schematic illustration of the photocatalytic process of GFO/H_2O_2 system for the degradation of organic contaminations in aqueous solution

$$\equiv Fe^{III} + H_2O_2 \rightarrow \equiv Fe^{II} + {}^{\cdot}OOH + H^+ \quad (1)$$

$$\equiv Fe^{III} + {}^{\cdot}OOH \rightarrow \equiv Fe^{II} + O_2 + H^+ \quad (2)$$

$$\equiv Fe^{II} + H_2O_2 \rightarrow \equiv Fe^{III} + {}^{\cdot}OH + OH^- \quad (3)$$

In the present GFO–H_2O_2 system, the heterogeneous Fenton-like reaction between the sample and H_2O_2 had occurred before illumination, which can be clearly observed from the two initial absorbances at $t = 0$ (Fig. 4a, b). After maintaining the suspensions in the dark for 30 min to establish an adsorption/desorption equilibrium, the initial absorbance decreased obviously (18.9 %) when hydrogen peroxide was present. It is implied that $GdFeO_3$ is actually acting as heterogeneous Fenton-like catalyst [29]. When a small amount of H_2O_2 was introduced into the photoreaction suspension, the interfacial Fe atoms (denoted as $\equiv Fe^{III}$) of $GdFeO_3$ nanoparticles with the extremely high surface potential could react with H_2O_2 to form $^{\cdot}OH$ radicals through Fenton-like reaction (Eqs. 1–3). Meanwhile, under visible-light illumination, photogenerated electron–hole pairs formed in GFO nanoparticles. Thus, the electrons were easily trapped by the H_2O_2 forming $^{\cdot}OH$ radicals. The obvious enhancement in the efficiency of RhB removal with the addition of H_2O_2 may be ascribed to the synergistic effect of semiconductor-photocatalyzed oxidation and heterogeneous Fenton-like reaction. The schematic illustration of the photogeneration of electron–hole pairs and the photocatalysis process of RhB over GFO is depicted in Fig. 5.

The photocatalytic mechanism of GFO composites was further revealed by the trapping experiments to determine the main active species in the photocatalytic process. It is well known that the decomposition of dyes over photocatalyst is mainly ascribed to photogenerated reactive species such as h^+, $O_2^{\cdot-}$, $^{\cdot}OOH$ and $^{\cdot}OH$, and so on [40, 41]. The degradation of RhB can be increased greatly when adding small H_2O_2 as electron scavenger, indicating photogenerated electrons play a vital role in photocatalysis.

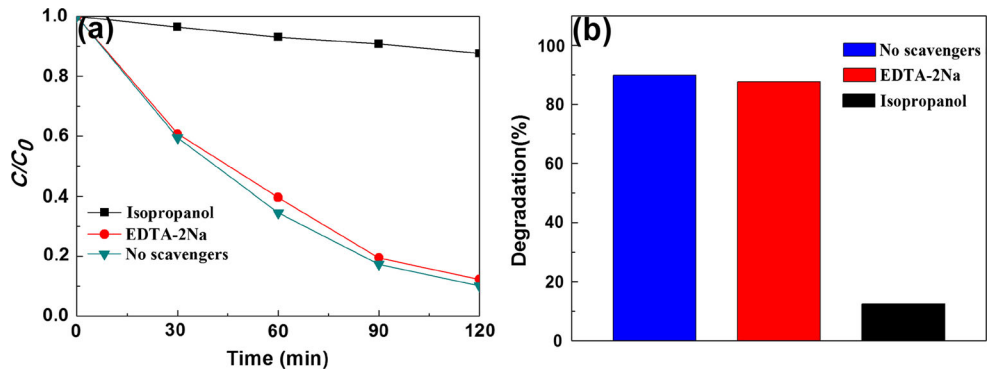

Fig. 6 **a** Photocatalytic activities of GFO/H_2O_2 system for the degradation of RhB in the presence of different scavengers. **b** The corresponding photodegradation efficiencies of RhB illuminated for 120 min

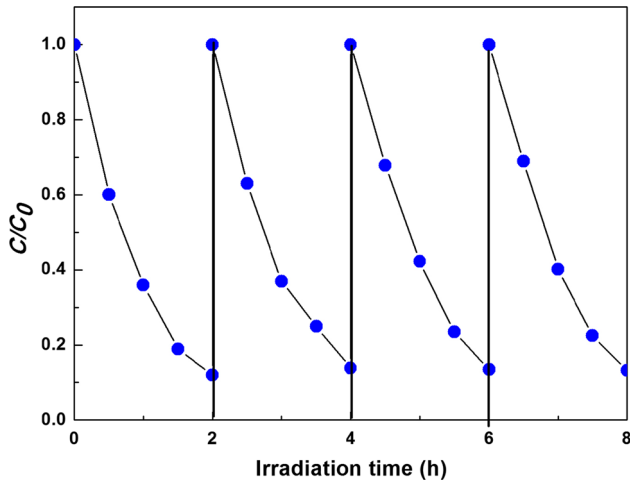

Fig. 7 Recycling test on the GFO/H_2O_2 system for the degradation of RhB under visible-light irradiation

Disodium ethylenediaminetetraacetate (EDTA-2Na) and isopropanol were used as holes and ·OH radical scavenger, respectively. As shown in Fig. 6a, the degradation of RhB was slightly inhibited in the presence of EDTA-2Na, revealing that the photogenerated holes are not the main active species for RhB degradation. When isopropanol is added into the reaction solution, the photocatalytic reaction is strongly suppressed, indicating that ·OH radicals are responsible for the degradation process. From Fig. 6b, the photocatalytic degradation efficiency of RhB was 89.9 % in 2 h without any scavengers. When EDTA-2Na and isopropanol were added, it can reach to 87.7 and 12.4 %, respectively. Therefore, it confirmed that reactive oxygen species (·OH or/and ·OOH) play the dominant roles in RhB photodegradation over GFO/H_2O_2 system.

In addition to the photocatalytic efficiency, the catalyst's lifetime is another important parameter of the photocatalytic process, so it is essential to evaluate the stability of the catalyst for practical application. The cycling runs for RhB photodegradation over GFO were performed, and the result was displayed in Fig. 7. Only a slight decrease was observed after four recycling runs, which can be attributed to the loss of catalyst during the recycle process. Obviously, the prepared GFO photocatalyst showed good stability during the photocatalytic reaction with the aid of H_2O_2.

4 Conclusions

In summary, $GdFeO_3$ photocatalyst was successfully prepared with by a glycine-assisted auto-combustion method. The study evaluated the performance of GFO/H_2O_2 as a heterogeneous Fenton-like system for the oxidation of RhB in water. The results indicated that GFO/H_2O_2 can degrade RhB more effectively than either H_2O_2 oxidation or GFO degradation alone. The enhanced removal can be ascribed to the formation of ·OH that rapidly degrades the target compound. The trapping experiments indicated that the hydroxyl radicals played the dominant roles in RhB photodegradation over the GFO/H_2O_2 system again. These encouraging data demonstrate that the GFO/H_2O_2 system has potential applications in organic pollution treatment.

Acknowledgments We gratefully acknowledge the financial supports from the NSFC (21001064), the Natural Science Foundation of Jiangsu Province (BK2010487), the key Science Foundation of Huainan Normal University (2014xk10zd), the key Natural Science Foundation of Anhui Province (KJ2015A160), the key excellent young talents foundation of Anhui Province (gxyqZD2016262), and the Natural Science Foundation of Anhui Province (1408085QB23).

References

1. Li HP, Liu JY, Hou WG, Du N, Zhang RJ, Tao XT (2014) Synthesis and characterization of g-C_3N_4/Bi_2MoO_6 heterojunctions with enhanced visible light photocatalytic activity. Appl Catal B Environ 160–161:89–97
2. McFarland EW, Metiu H (2013) Catalysis by doped oxides. Chem Rev 113:4391–4427
3. Ye L, Tian L, Peng T, Zan L (2011) Synthesis of highly symmetrical BiOI single-crystal nanosheets and their 001 facet-dependent photoactivity. J Mater Chem 21:12479–12484
4. Paracchino A, Laporte V, Sivula K, Grätzel M, Thimsen E (2011) Highly active oxide photocathode for photoelectrochemical water reduction. Nat Mater 10:456–461
5. Chen DM, Kuang Z, Zhu Q, Du Y, Zhu HL (2015) Synthesis and characterization of CdS/$BiPO_4$ heterojunction photocatalyst. Mater Res Bull 66:262–267
6. Shi R, Wang Y, Li D, Xu J, Zhu YF (2010) Synthesis of $ZnWO_4$ nanorods with [100] orientation and enhanced photocatalytic properties. Appl Catal B 100:173–178
7. Pan C, Zhu Y (2010) New type of $BiPO_4$ oxy-acid salt photocatalyst with high photocatalytic activity on degradation of dye. Environ Sci Technol 44:5570–5574
8. Li GF, Ding Y, Zhang YF, Lu Z, Sun HZ, Chen R (2011) Microwave synthesis of $BiPO_4$ nanostructures and their morphology-dependent photocatalytic performances. J Colloid Interface Sci 363:497–503
9. Fu J, Chang BB, Tian YL, Xi FN, Dong XP (2013) Novel C_3N_4–CdS composite photocatalysts with organic–inorganic heterojunctions: in situ synthesis, exceptional activity, high stability and photocatalytic mechanism. J Mater Chem A 9:3083–3090
10. Chen T, Zhou ZL, Wang YD (2009) Surfactant CATB-assisted generation and gas-sensing characteristics of $LnFeO_3$ (Ln = La, Sm, Eu) materials. Sens Actuators, B 143:124–131
11. Asamoto M, Iwasaki Y, Yamaguchi S, Yahiro H (2012) Synthesis of perovsite-type oxide catalysts, Ln(Fe, Co)O_3 (Ln = La, Pr, Sm, Gd, Dy, Ho, Er, and Yb) from the thermal decomposition of the corresponding cyano complexes. Catal Today 185:230–235
12. Hosoya Y, Itagaki Y, Aono H, Sadaoka Y (2005) Ozone detection in air using $SmFeO_3$ gas sensor. Sens Actuators, B 108:198–201
13. Ding JL, Lü XM, Shu HM, Xie JM, Zhang H (2010) Microwave-assisted synthesis of perovskite $ReFeO_3$ (Re: La, Sm, Eu, Gd) photocatalyst. Mater Sci Eng, B 171:31–34

14. Tang PS, Tong Y, Chen HF, Cao F, Pan GX (2013) Microwave-assisted synthesis of nanoparticulate perovskite $LaFeO_3$ as a high active visible-light photocatalyst. Curr Appl Phys 13:340–343
15. Jiang LW, Liu WL, Wu AH, Xu J, Liu Q, Qian GX, Zhang HJ (2012) Low-temperature combustion synthesis of nanocrystalline $HoFeO_3$ powders via a sol-gel method using glycin. Ceram Int 38:3667–3672
16. Siemons M, Leifert A, Simon U (2007) Preparation and gas sensing characteristics of nanoparticulate p-type semiconducting $LnFeO_3$ and $LnCrO_3$ materials. Adv Funct Mater 17:2189–2198
17. Xu H, Hu XL, Zhang LZ (2008) Generalized low-temperature synthesis of nanocrystalline rare-earth orthoferrites $LnFeO_3$ (Ln = La, Pr, Nd, Sm, Eu, Gd). Cryst Growth Des 8:2061–2065
18. Li L, Wang X, Zhang YG (2014) Enhanced visible light-responsive photocatalytic activity of $LnFeO_3$ (Ln = La, Sm) nanoparticles by synergistic catalysis. Mater Res Bull 50:18–22
19. Lü XM, Xie JM, Shu HM, Liu J, Yin CQ, Lin JM (2007) Microwave-assisted synthesis of nanocrystalline $YFeO_3$ and study of its photoactivity. Mater Sci Eng, B 138:289–292
20. Ju LL, Chen ZY, Fang L, Dong W, Zheng FG, Shen MR (2011) Sol–gel synthesis and photo-Fenton-like catalytic activity of $EuFeO_3$ nanparticles. J Am Ceram Soc 10:3418–3424
21. Sun SM, Wang WZ, Zhong L, Shang M (2009) Visible light-induced photocatalytic oxidation of phenol and aqueous ammonia in flowerlike $Bi_2Fe_4O_9$ suspensions. J Phys Chem C 113: 12826–12831
22. Thirumalairajan S, Girija K, Mastelaro VR, Ponpandian N (2014) Photocatalytic degradation of organic dyes under visible light irradiation by floral-like $LaFeO_3$ nanostructures comprised of nanosheet petals. New J Chem 38:5480–5490
23. Navarro MC, Pannunzio-Miner EV, Pagola S, Gómez MI, Carbonio RE (2005) Structural refinement of $Nd[Fe(CN)_6]\cdot 4H_2O$ and study of $NdFeO_3$ obtained by its oxidative thermal decomposition at very low temperatures. J Solid State Chem 178:847–852
24. Li X, Tang CJ, Ai M, Dong L, Xu Z (2010) Controllable synthesis of pure-phase rare-earth orthoferrites hollow spheres with a porous shell and their catalytic performance for the CO + NO reaction. Chem Mater 22:4879–4884
25. Wu L, Yu JC, Zhang LZ, Wang XC, Li SK (2004) Selective self-propagating combustion synthesis of hexagonal and orthorhombic nanocrystalline yttrium iron oxide. J Solid State Chem 177:3666–3674
26. Chavan SV, Tyagi AK (2005) Nanocrystalline $GdFeO_3$ via the gel-combustion process. J Mater Res 10:2654–2660
27. Li X, Duan ZQ (2012) Synthesis of $GdFeO_3$ microspheres assembled by nanoparticles as magnetically recoverable and visible-light-driven photocatalysts. Mater Lett 89:262–265
28. Wang X, Mao HM, Shan YC (2014) Enhanced photocatalytic behavior and excellent electrochemical performance of hierarchically structured NiO microspheres. RSC Adv 4:35614–35619
29. Wang X, Zhang M, Tian P, Chin WS, Zhang CM (2014) A facile approach to pure-phase $Bi_2Fe_4O_9$ nanoparticles sensitive to visible light. Appl Surf Sci 321:144–149
30. Paola AD, García-López E, Marcì G, Palmisano L (2012) A survey of photocatalytic materials for environmental remediation. J Hazard Mater 211–212:3–29
31. Li L, Wang X, Lan Y, Gu W, Zhang SL (2013) Synthesis, photocatalytic and electrocatalytic activities of wormlike $GdFeO_3$ nanoparticles by a glycol-assisted sol–gel process. Ind Eng Chem Res 52:9130–9136
32. Wang X, Tian P, Lin Y, Li L (2015) Hierarchical nanostructures assembled from ultrathin Bi_2WO_6 nanoflakes and their visible-light induced photocatalytic property. J Alloys Compd 620: 228–232
33. Yang XF, Cui HY, Li Y, Qin JL, Zhang RX, Tang H (2013) Fabrication of Ag_3PO_4-graphene composites with highly efficient and stable visible light photocatalytic performance. ACS Catal 3:363–369
34. Fu GK, Xu GN, Chen SP, Lei L, Zhang ML (2013) Ag_3PO_4/Bi_2WO_6 hierarchical heterostructures with enhanced visible light photocatalytic activity for the degradation of phenol. Catal Commun 40:120–124
35. Luo W, Zhu LH, Wang N, Tang HQ, Cao MJ, She YB (2010) Efficient removal of organic pollutants with magnetic nanoscaled $BiFeO_3$ as a reusable heterogeneous Fenton-like catalyst. Environ Sci Technol 44:1786–1791
36. Wang X, Lin Y, Ding XF, Jiang JG (2011) Enhanced visible-light-response photocatalytic activity of bismuth ferrite nanoparticles. J Alloys Compd 23:6585–6588
37. Lan HC, Wang AM, Liu RP, Liu HJ, Qu JH (2015) Heterogeneous photo-Fenton degradation of acid red B over Fe_2O_3 supported on activated carbon fiber. J Hazard Mater 285:167–172
38. Zou L, Wang X, Xu XY, Wang HR (2016) Reduced graphene oxide wrapped CdS composites with enhanced photocatalytic performance and high stability. Ceram Int 42:372–378
39. Li L, Wang HR, Zou L, Wang X (2015) Controllable synthesis, photocatalytic and electrocatalytic properties of CeO_2 nanocrystals. RSC Adv 5:41506–41512
40. Lima LVC, Rodriguez M, Freitas VAA, Souza TE, Machado AEH, Patrocínio AOT, Fabris JD, Oliveirab LCA, Pereira MC (2015) Synergism between n-type WO_3 and p-type α-FeOOH semiconductors: high interfacial contacts and enhanced photocatalysis Lucas. Appl Catal B Environ 165:579–588
41. Xiang QJ, Lang D, Shen TT, Liu F (2015) Graphene-modified nanosized Ag_3PO_4 photocatalysts for enhanced visible-light photocatalytic activity and stability. Appl Catal B Environ 162:196–203